Adsorption Configurations and Reactions of Boric Acid on a TiO_2 Anatase (101) Surface

P. Raghunath[†] and M. C. Lin*[,†,‡]

Center for Interdisciplinary Molecular Science, Institute of Molecular Science, National Chiao Tung University, Hsinchu 300, Taiwan, and Department of Chemistry, Emory University, Atlanta, Georgia 30322

Received: November 28, 2007; Revised Manuscript Received: March 10, 2008

This study investigates the adsorption and reactions of the monomer and dimer of $B(OH)_3$ on a TiO_2 anatase (101) surface by first-principles calculations based on the density functional theory and pseudopotential method. On the clean surface, the most stable adsorption structure for $B(OH)_3$ is a molecular monodentate configuration with one hydrogen bonded to a neighboring surface bridging oxygen. The adsorbed $B(OH)_3$ molecule can dissociate into the bidentate adsorption configuration, Ti−OB(OH)O−Ti(a), in which the −OB(OH)O− moiety binds to the surface through two Ti−O bonds with the two dissociated H atoms on neighboring bridged surface oxygen atoms following two successive H migrations. The overall exothermicity is 10.8 kcal/mol; significantly the adsorption energy for Ti−OB(OH)O−Ti(a) with 2 H's on two O_{2c} surface atoms is 140.1 kcal/mol. In the case of the dimer, there are two identical molecules like the monodentate configuration of $B(OH)_3$ adsorbed on two 5-fold-coordinated Ti atoms of the surface. The Ti−OB(OH)OB(OH)O−Ti binding with 2 H's on two neighboring O_{2c} surface atoms is very strong like the monomer case, with 150.0 kcal/mol of adsorption energy. Thus, both Ti−OB(OH)O−Ti and Ti−OB(OH)OB(OH)O−Ti adsorbates can be employed as strong linkers between semiconductor quantum dots such as InN and TiO_2 nanoparticles. The energeties and mechanisms of these surface reactions have also been explicitly predicted with the computed potential energy surfaces. Most of the $B(OH)_3$ reactions on the anatase surface are exothermic.

1. Introduction

The titanium dioxide (TiO_2) nanoparticle film is a polycrystalline material with different TiO_2 surface structures. The (101) and (110) surfaces of anatase and rutile, respectively, have lower energies with similar characteristics; they may coexist in the nanoparticle film.[1] The photophysics of TiO_2 sensitized by dyes,[2,3] polymers,[4,5] and semiconductors[6,7] has been widely studied, with an aim of solar energy conversion by the photovoltaic effect. Dye-sensitized TiO_2 photovoltaic solar cells, which exhibit an energy conversion efficiency of around 10%, were successfully pioneered by Graetzel and co-workers.[2,3] However, efficient dyes are very expensive,[8] and organic compounds have shorter lifetimes as well as being less stable than inorganic semiconductive materials, which may be directly employed for H_2O splitting. Among these semiconductors, quantum dot (QD)-sensitized TiO_2 nanoparticles (by InP, InAs, PbS, and CdS, for example) have been well-examined [6,7] and showed evidence of electron transfer from quantum dots into the TiO_2 nanoparticles. We have done experimental and theoretical studies on the deposition of InN films of varying thickness on TiO_2 nanoparticle films fabricated by low-pressure organometallic chemical vapor deposition (OMCVD) near 700 K with continuous UV irradiation using hydrazoic acid (HN_3) and trimethylindium (TMIn), which are perhaps the most efficient precursors.[9–11] The resulting InN films on TiO_2 exhibit a broad UV/visible absorption between 390 and 800 nm, indicating a promising possibility for photovoltaic applications.[10a] For both dye- and QD-sensitized metal oxide solar cells, the anchoring group between the sensitizer and the metal oxide film plays a critical role. Interaction of anchoring groups (COO^- and $-PO_3^{2-}$) with different metal oxide surfaces has been a subject of several experimental and theoretical studies.[12]

Recently, Wang[13] experimentally observed the effects of surface modifiers, such as boric acid $B(OH)_3$ and phosphorous acid $P(OH)_3$, on the photocurrent generated by InN/TiO_2 nanoparticle films. The result shows an enhancement in power conversion efficiency by boric acid treatment, whereas phosphorous acid treatment exhibits a negative effect on the photocurrent conversion efficiency. To understand the effects, in this study, we calculate the stability of boric acid and the dissociation products on anatase TiO_2 (101), which is the primary phase of TiO_2 in the film prepared by the sol−gel method.[9a] Chang et al. recently investigated the adsorption and reactions of boron trichloride and its fragments (BCl_x) on the TiO_2 anatase (101) and rutile (110) surfaces by first-principles calculations.[14] Adsorption of HCOOH and H_3PO_3 on the surfaces of a TiO_2 anatase (101) surface has been extensively studied theoretically.[12f,15]

The main aim of this work is to investigate the adsorption and reaction pathways of the monomer and dimer of boric acid on the TiO_2 anatase (101) surface by first-principles calculations and to identify the key stable species which may potentially serve as a linker between the InN and TiO_2 in the experiment.[13] This type of model calculation allows us to construct more complete potential energy surfaces for simulation of surface reactions and to predict the hydrogen effect on the adsorbates. In section 2, we describe the computational method employed in the current study. The computational results, which include the optimized adsorbate structures, adsorption energies, potential energy surfaces, hydrogen coadsorption effect, and Bader atomic charges, are reported in section 3. The calculated geometries and adsorption energies are expected to be helpful for the likely

* To whom correspondence should be addressed. E-mail: chemmcl@emory.edu.
† National Chiao Tung University.
‡ Emory University.

10.1021/jp711246b CCC: $40.75
Published on Web 05/07/2008

identification of the new anchoring groups for the fabrication of solar cells.

2. Computational Details

The geometrical structures are optimized by the Vienna ab initio simulation package (VASP),[16–19] implementing the density functional theory. The exchange−correlation function was treated with the local-density approximation (LDA).[20] The generalized gradient approximation (GGA)[21,22] used for the total energy calculations was that of the spin-polarized Perdew−Wang 1991 (PW91)[21] formulation, which has been shown to work well for surfaces.[23] For the present calculation, the interaction between ions and electrons is described using ultrasoft Vanderbilt pseudopotentials (US-PP) supplied by VASP. The 10 3p, 3d, and 4s electrons of each Ti atom and 6 2s and 2p electrons of each O atom were explicitly considered. For the periodic condition, the electronic orbitals are explained by a plane-wave basis set. The plane-wave expansion includes all plane waves with their kinetic energies smaller than the chosen cutoff energy, $\hbar k^2/2m < E_{cut}$, which ensures the convergence with respect to the basis set. In all of our calculations, we used a 500 eV cutoff energy. The Brillouin zone was sampled with the chosen Monkhorst−Pack *k*-points,[24] which also ensure the convergence of the whole system. The transition states for dissociative adsorptions were found using the climbing-image nudged elastic band method (CI-NEB).[25,26] All transition-state structures were characterized by calculating the vibrational frequencies. The structure and bond length of the different isomers of gas-phase molecules of $B(OH)_3$ were calculated by VASP and Gaussian 03[27] and their fragments by VASP.

In the present calculations, the slab model was adopted to simulate the interaction between the TiO_2 anatase (101) surface and $B(OH)_3$. The slab cell employed for TiO_2 anatase calculations contains 24 [TiO_2] units. In the direction perpendicular to the *Z*-axis of the super cell, a vacuum space (17.8 Å) of a sufficient separation was imposed for the surface reaction as well as to ensure no interaction with the lowest layer of the upper slab. The lowest layer of the super cell was fixed in the calculation to prevent surface deformation. Gas-phase atoms and molecules were simulated in a box 20 Å on a side, large enough to ensure negligible interactions between neighboring cells. The adsorption energy, E_{ads}, was calculated according to the expression

$$E_{ads} = E_{slab} + E_{molecule} - E_{(slab+molecule)}$$

where E_{slab} represents the energy of the clean slab, $E_{molecule}$ is the energy of the adsorbate in the gas phase, and $E_{(slab+molecule)}$ is the total energy of the slab with adsorbate. In the case of coadsorption of an adsorbate with H, to estimate the adsorption energy of the adsorbate, we used

$$E_{ads} = E_{slab/H} + E_{molecule} - E_{(slab/H+molecule)}$$

where $E_{slab/H}$ represents the energy of the slab covered with H in the coadsorption configuration and $E_{(slab/H+molecule)}$ is the total energy of the slab with the adsorbate and H coadsobed on it. Spin-polarized calculations were carried out throughout the system. A positive value of $E_{ads} > 0$ indicates stable adsorption. Atomic charges of the optimized structures were computed using the Bader method with a program by Henkelman et al.[28] For the Bader charge analyses, the adsorbate structures were optimized by using the projector augmented wave (PAW) potential. With this program, we can calculate the atomic charges of the optimized structures to examine the charges transfer between adsorbates and the substrate.

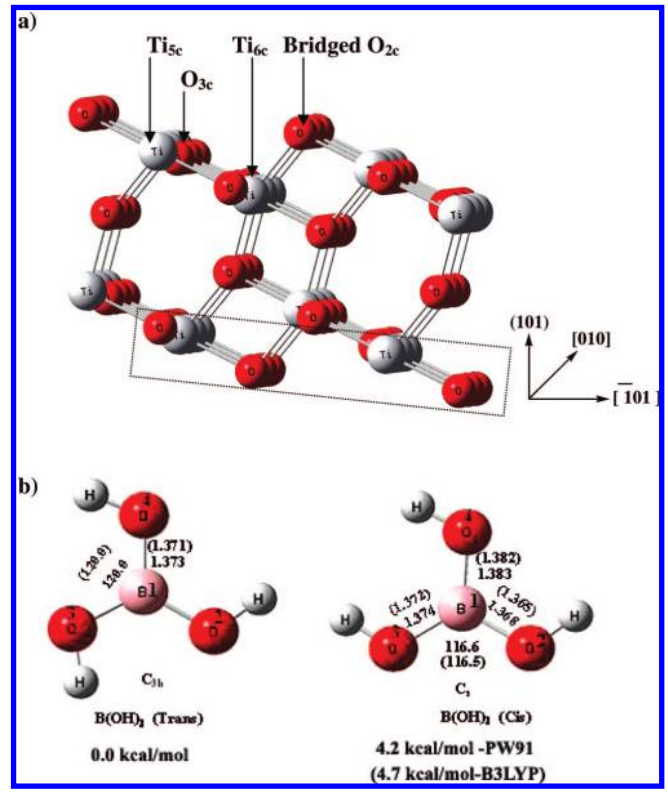

Figure 1. a) Perspective view of the TiO_2 anatase (101) surface slab model used in the present study. The dashed lines indicate the fixed atoms in the slab calculations. b) Optimized structures of two isomers of $B(OH)_3$ calculated using the PW91 level and B3LYP/6-31G(d,p) methods.

3. Results and Discussion

3.1. Verification. To ensure the reliability of the computational results, the method and parameters employed in the current study have first been examined by optimizing the bulk TiO_2 in the anatase phase, which is tetragonal, and by characterizing its lattice constants *a* and *c*. Flat anatase (101) terraces exhibit a sawtooth-like surface structure shown in Figure 1a. It is characterized by the presence of acidic−basic pairs of coordinative unsaturated ions, that is, five-fold-coordinated Ti^{4+} ions (Ti_{5c}) and two-fold-coordinated bridging oxygen O^{2-} ions (O_{2c}) including coordinated ions on the surface (O_{3c}, Ti_{6c}). The two-fold-coordinated O atoms and five-fold-coordinated Ti atoms are more active because the lower coordination of these atoms binds more strongly with adsorbates. Experimental bulk lattice parameters of the anatase surface are $a = 3.782$ Å and $c = 9.502$ Å.[29] The model-size 3 × 1 × 2 super cell used for our simulations with the $Ti_{24}O_{48}$ composition and the surface was 11.355 Å × 10.24 Å, separated perpendicularly by the 17.8 Å vacuum space. The parameters for the 2 × 2 × 1 Monkhorst−Pack *k*-points and 500 eV cutoff energy were used in the present calculations. The $O_{2c}(O_{3c})$ moves into (out of) the surface by 0.025 Å (0.220 Å). Similarly, the Ti_{5c} and Ti_{6c} move into and out of the surface by 0.154 and 0.169 Å, respectively. The results of surface atom displacement are in good agreement with previous results.[30,31]

Testing the Model. We have tested the reliability of this surface model by computing the adsorption energies of H_2O and HCOOH on the surface; they are presented in Table 1, and their structures are given in Figure 2.

Adsorption of H_2O. The adsorption energy of water on TiO_2(101) was obtained as 19.2 kcal/mol, which is close to the experimental range, 11.5−16.1 kcal/mol.[30,32] Figure 2b shows

TABLE 1: Optimized Bond Lengths (Å) and Adsorption Energies (kcal/mol) for H_2O and HCOOH and Its Fragments on the TiO_2 (101) Surface

structure	Ti−O1	O1H−O_b	O1−HO_b	O_b−Ti_{6c}	E_{ads}
H_2O−Ti(a)	2.275	2.094		1.899	19.2
H_2O−Ti(a)[a]	2.275	2.374		2.164	18.6
HO−Ti(a)	1.851			1.881	24.9
HO−Ti(a)[a]	1.870		2.330	2.081	75.0

structure	Ti−O1	O1−C2	C2−O3	O3−Ti	O3H−O_b	O_b−Ti_{6c}	E_{ads}
Ti−OC(H)OH···O_b(a)	2.129	1.240	1.298		1.505	1.937	21.9
Ti−OC(H)O−Ti(a)	2.119	1.269	1.269	2.119		1.892	23.5
Ti−OC(H)O−Ti(a)[a]	2.104	1.274	1.268	2.087		2.136	72.9

[a] The adsorption is on the surface with one H(a) adsorbed on the anatase TiO_2(101) surface ($^aE_{ads} = E_{slab/H} + E_{molecule} - E_{(slab/H+molecule)}$).

the adsorption of H_2O on the Ti_{5c} and H atom on the bridged surface oxygen; their adsorption energy is 18.6 kcal/mol. Molecular adsorption of H_2O, followed by dissociation, gives OH^- attached by its oxygen end to the Ti_{5c} and H^+ bonded to lattice oxygen to form a hydroxyl group (see Figure 2c). H_2O dissociation on the surface produces OH on the Ti_{5c} site and H on a neighboring bridging oxygen, with the energy lying 7.74 kcal/mol below the $H_2O(g) + TiO_2$, which is in agreement with previously published DFT results (6.9 kcal/mol).[30] The adsorption energy for coadsorption of OH with H on the bridged surface is 75.0 kcal/mol. For OH at Ti_{5c} sites on the clean surface, we found an adsorption energy of 24.9 kcal/mol.

Adsorption of HCOOH. The $HCOO^-$ group has been employed as the anchoring group of dye-sensitized solar cells. Recently, Vittadini et al. have studied the adsorption of HCOOH on the TiO_2 anatase (101) surface by first-principles calculations based on DFT.[15] In agreement with those studies, we find the molecular adsorption and dissociative adsorption configurations of HCOOH geometries and parameters, shown in Figure 2. The stable HCOOH molecule binds to the surface Ti_{5c} via an O−Ti_{5c} bond and one H bond with a nearby surface O_{2c}; its adsorption energy is 21.9 kcal/mol (see Figure 2e). Dissociation of HCOOH on the surface produces a bidentate bridging configuration of the HC(O)O on the two Ti_{5c} sites and H on the bridging oxygen lying 20 kcal/mol below the $HCOOH(g) + TiO_2$ (see Figure 2f). The adsorption energy for the stable configuration of the formate ligand on the surface is 23.5 kcal/mol (see Figure 2g). The most favorable bidentate-bridged configuration of HC(O)O binding is with two Ti_{5c} sites and coadsorption with a H atom at a bridged oxygen; its adsorption energy is 72.9 kcal/mol (see Figure 2f). The detailed bond lengths are given in the Table 1. This Ti_{6c}−O_b bond length is significantly longer than that associated with the chemisorption bonds of formate (2.087 Å) and hydroxyl (2.136 Å) on this surface, whereas that with the Ti_{6c}−O_b bond length in the Ti−OC(H)O−Ti (a) is 1.892 Å. Experimentally, the scanned-energy mode photoelectron diffraction (PhD) technique[33e] has been used to investigate the structure of coadsorbed formate ($HCOO^-$) and hydroxyl (OH) species on TiO_2(110) produced by the reaction of formic acid on the surface.[33] The Ti−O distance associated with the formate bonding and Ti−O of these hydroxyl species are 2.08 and 2.02 Å, respectively, which are in good agreement with our results.

3.2. Potential Energy Surfaces and Reaction Mechanism. ***Reactions of B(OH)$_3$ Adsorbates on Anatase.*** The optimized structure and geometrical parameters of the isolated $B(OH)_3$ molecule in the gas phase is shown in Figure 1b. The stable structure belongs to C_{3h} symmetry in the trans conformation of each of the three O−H groups. We have also obtained the C_s symmetry structure, optimized as the cis conformation of two O−H groups. The cis structure is 4.2 (4.7) kcal/mol less stable than the trans structure by the PW91 (B3LYP/6-31G(d,p)) method, in good agreement with the previous theoretical value of 4.8 kcal/mol by the B3LYP method.[34]

Adsorption of B(OH)$_3$. The adsorption characteristics of orthoboric acid on the six-layer TiO_2 slab were mapped out by the DFT computation. In this study, we calculated several different bonding possibilities for an adsorbate that binds with the metal oxide surface. The coordination may be either monodentate or bidentate, depending on the number of oxygens used by the molecule/anion to coordinate with the surface Ti_{5c} acid sites. The possible most stable adsorption configurations of $B(OH)_3$ and its fragments on the TiO_2 anatase (101) surface are shown in Figure 3, and the associated bond lengths and adsorption energies are also listed in Table 2. The energies are all referenced to the initial reactants, $B(OH)_3(g) + TiO_2$ anatase (101) surface. In this study, we obtained the two most stable adsorbate structures. On the clean surface, the most stable adsorption structure for $B(OH)_3$ is a molecular monodentate configuration with one hydroxyl oxygen attached to a surface Ti_{5c} atom and another hydroxyl group to form a hydrogen bond to the doubly coordinated bridge surface oxygen (O_{2c}) atom denoted by O_b···HOB(OH)O(H)−Ti(a) in Figure 3a. Its adsorption energy is 17.2 kcal/mol, and in this structure, the Ti_{5c}−O bond length is 2.279 Å, and the OH−O_{2c} bond length is 1.658 Å, as given in Table 2. The next lowest-energy conformation is a bidentate configuration, where two adsorbate hydroxyl oxygens are binding to two surface Ti_{5c} atoms with an adsorption energy of 13.5 kcal/mol. Ti−O(H)B(OH)O(H)−Ti(a) bond lengths are slightly increased; two of the Ti_{5c}−O bond lengths are 2.436 and 2.431 Å (see Figure 3b). Another conformation of $B(OH)_3$ has a lower adsorption energy; boron is interacting with bridging oxygen with 6.2 kcal/mol of energy, and its geometry is given in the Supporting Information. The results indicate that monodentate and bidentate bridge binding modes are energetically quite favorable, with a rather small difference in adsorption energies. The dissociative reactions of monomer $B(OH)_3$ on the surface potential energy surface are divided into two types involving the two stable monodentate and bidentate adsorbates.

Reaction Path for the Adsorption and Dissociation of B(OH)$_3$ on the Surface. The computed potential energy surface of dissociative adsorption reactions of $B(OH)_3$ on the clean anatase (101) surface is shown in Figures 4 and 5. The optimized structures depicted with the surface model are presented in Figure 3, and selected bond lengths are listed in Table 2. First, as alluded to above, the most stable monodentate adsorption reactions are calculated. One of the OH group's lone-pair electrons of its oxygen can molecularly adsorb on an unsaturated surface Ti_{5c} atom, giving O_b···HOB(OH)O(H)−Ti(a) with an

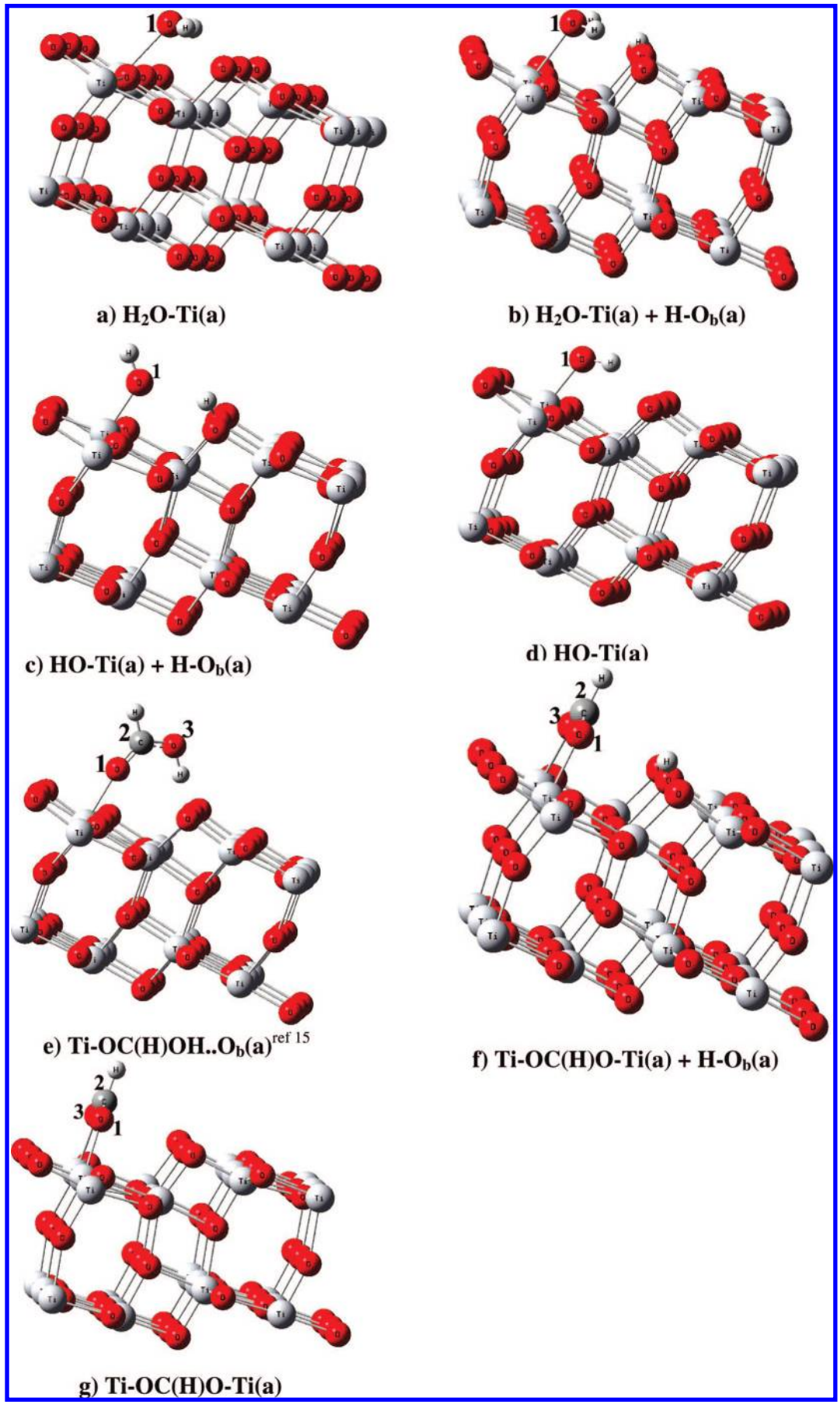

Figure 2. Optimized structures of possible adsorbed and dissociatively adsorbed H_2O and HCOOH on the anatase TiO_2(101) surface.

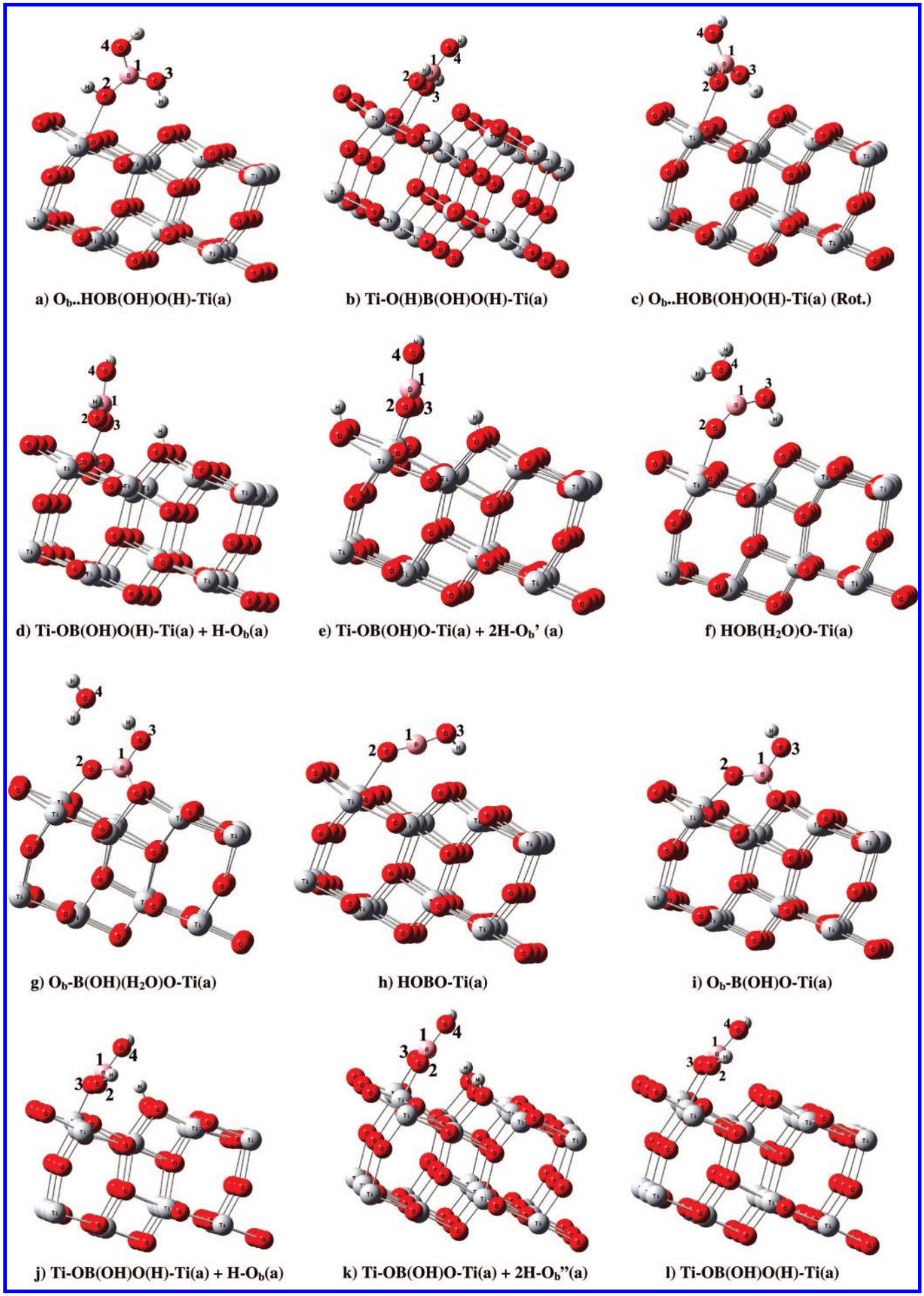

Figure 3. Part 1 of 2.

Figure 3. Part 2 of 2. Optimized structures of possible adsorbed and dissociatively adsorbed $B(OH)_3$ on the anatase (101) surface presented in Figures 4 and 5. (The ′ represents the two hydrogens adsorbed on the different sides of the bridged oxygen row; see (e). The ″ represents the two hydrogens adsorbed on the same side of the bridged oxygen row; see (k).)

TABLE 2: Optimized Bond Lengths (Å) and Adsorption Energies (kcal/mol) for $B(OH)_3$ and Its Fragments on the TiO_2(101) Surface

structure	Ti−O2	O2−B1	B1−O3	B1−O4	Ti−O3	B1−O_b	OH−O_b	O_b−Ti_{6c}	E_{ads}
O_b···HOB(OH)O(H)−Ti(a)	2.279	1.413	1.340	1.374	−	−	1.658	1.904	17.2
Ti−O(H)B(OH)O(H)−Ti(a)	2.436	1.386	1.391	1.365	2.431	−		1.894	13.5
O_b···HOB(OH)O(H)−Ti(a) (rot)	2.379	1.414	1.358	1.368	1.358		1.694	1.910	12.0
Ti−OB(OH)O(H)−Ti(a)	2.276	1.428	1.350	1.371	1.925			1.887	28.0
Ti−OB(OH)O(H)−Ti(a)[a]	2.306	1.428	1.343	1.378	1.935			2.116	74.9
Ti−OB(OH)O−Ti(a)	1.896	1.370	1.384	1.371	1.964			1.866	30.3
Ti−OB(OH)O−Ti(a)′[b]	1.846	1.384	1.377	1.375	1.902			2.118	140.1
HOBO−Ti(a)	2.169	1.229	1.299	−	−	−		1.918	21.7
O_b−B(OH)O−Ti(a)	1.917	1.363	1.370	−	−	1.430			44.1
H−O_b(a)	0.970							2.113	56.2
2H−O_b′(a)	0.975	0.975						2.132	109.1

[a] The adsorption is on the surface with one H(a) adsorbed on the anatase TiO_2(101) surface. [b] The adsorption is on the surface with two H(a) adsorbed on different sides on the anatase TiO_2(101) surface.

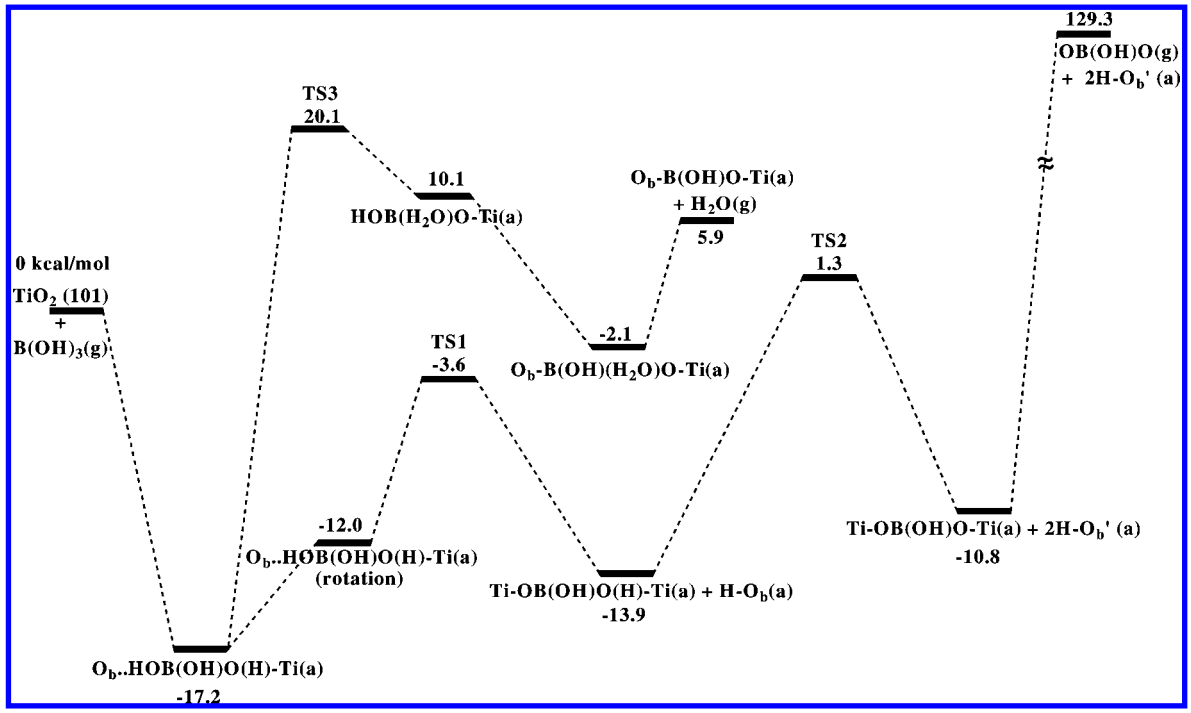

Figure 4. Potential energy surface of the surface reactions starting with the trans conformation of $B(OH)_3$(g) on the TiO_2(101) surface. (The ′ represents the two hydrogens adsorbed on the different sides of the bridged oxygen rows; see Figure 3e.)

adsorption energy of 17.2 kcal/mol. The dissociation of the monodentate adsorbate can take place in two ways. In one way, the hydrogen of the coordinating OH group can migrate to a neighboring O_{2c} which is exothermic, and the other reaction pathway is H_2O elimination from $B(OH)_3$(a), which is highly endothermic. Thus, this intermediate leads to two major dissociative adsorption products, Ti−OB(OH)O−Ti(a) + 2H−O_b′(a) and O_b−B(OH)O−Ti(a) + H_2O(g). Initially, the

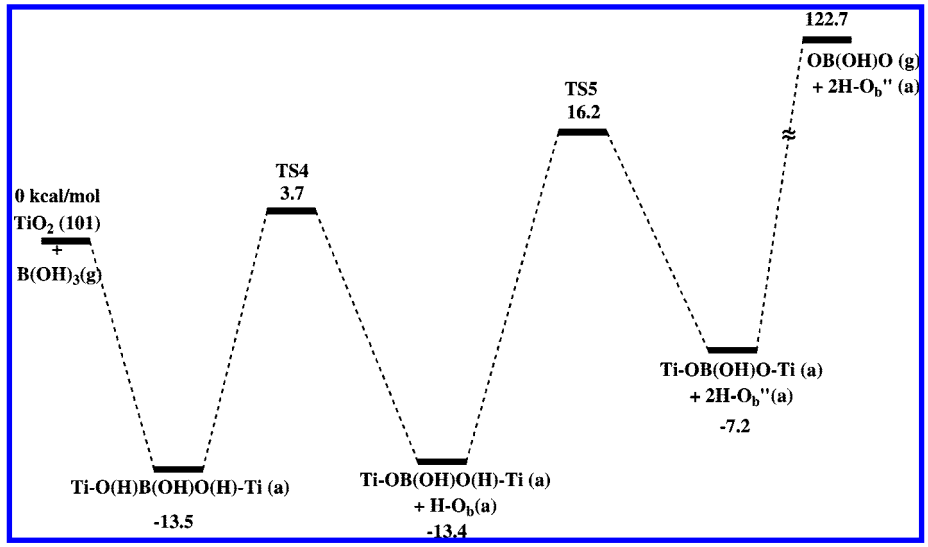

Figure 5. Potential energy surface of the surface reactions starting with the cis conformation of $B(OH)_3(g)$ on the $TiO_2(101)$ surface. (The ″ represents the two hydrogens adsorbed on the same side of the bridged oxygen rows; see Figure 3k.)

adsorbed boric acid molecularly can rotate on the surface. The required energy is 5.2 kcal/mol, and the bond length between Ti−O is increased by 0.1 Å. The rotated adsorbate HOB(OH)-O(H)−Ti(a) can then undergo cleavage of O−H bonds and results in the formation of a covalently bound Ti−OB-(OH)O(H)−Ti(a) species and H−O_b(a) (see Figure 3d). This dissociation reaction has an activation barrier lying 3.6 kcal/mol below the energy of the reactants. The transition state (**TS1**) of this channel takes place with the formation of the Ti_{5c}−O strong bond with a bond length of 1.935 Å, and the O_b-H length is 0.972 Å. The transition vector is dominated by the motion of the H atom in the dissociated OH group, which is 1.306 Å from the oxygen and 1.184 Å from the O_b. The transition-state geometries are given in the Supporting Information Figure S2. The exothermicity of the process is predicted to be 13.9 kcal/mol and converts the molecule from the monodentate to the bidentate conformation. Following the similar O−H bond cleavage process in the **TS1**, the Ti−OB(OH)O(H)−Ti(a) intermediate can also isomerize through a 15.2 kcal/mol barrier at **TS2**, and in the process H migrates from the −O(H)−Ti moiety to the closest O_b to produce Ti−OB(OH)O−Ti(a) + 2H−O_b′(a) with an exothermicity of 10.8 kcal/mol. According to the predicted coordination configuration, the Ti−OB(OH)-O−Ti(a) species can be bonded to the metal center via a bidentate bridging configuration, as illustrated in Figure 3e, with bond lengths of 1.846 and 1.902 Å between the Ti−O.

Another reaction pathway is that O_b···HOB(OH)O(H)−Ti(a) can produce the complex HOB(H_2O)O−Ti(a) (see Figure 3f). In this process, the H atom of the OH group binding with Ti can react with one of the OH groups to eliminate H_2O, producing HOB(H_2O)O−Ti(a) with 10.1 kcal/mol of endothermicity via **TS3** (activation barrier is 38.3 kcal/mol). The O−H bond length is 1.382 Å, and that for H−O is 1.166 Å. The intermediate complex thus formed has doubly coordinated B bonding to O_b, and Ti atoms lie 2.1 kcal/mol below the initial reactants. Finally, H_2O elimination from the surface molecular complex requires 8 kcal/mol of energy, and the final product O_b−B(OH)O−Ti(a) + H_2O(g) is 5.9 kcal/mol above the initial reactants.

The potential energy diagram for the dissociative adsorption of the cis conformation of boric acid on the anatase surface to form the bidentate adsorbate Ti−O(H)B(OH)O(H)−Ti(a) is shown in Figure 5. One of the O−H bonds binding with the surface can undergo H migration to a neighboring surface O_{2c} to form Ti−OB(OH)O(H)−Ti(a) + H−O_b(a) via **TS4** (17.2 kcal/mol), with their overall exothermicity computed to be 13.4 kcal/mol (see Figure 3j). Bond lengths between the O−Ti_{5c}, O−H, and H−O_b are 2.149, 1.343, and 1.226 Å, respectively. Following a similar proton migration as **TS4,** Ti−OB(OH)-O(H)−Ti(a) can form a Ti−OB(OH)O−Ti(a) + 2H−O_b″(a) (see Figure 3k) via a 29.6 kcal/mol barrier at **TS5.** In Ti−OB(OH)O−Ti(a), there is a strong binding between the two oxygens and surface Ti_{5c}, with slightly different Ti−O bond lengths, 1.877 and 1.864 Å. Finally, both potential energy surfaces (Figure 4 and 5) show that the desorption of OB(OH)O (g) from Ti−OB(OH)O−Ti(a) requires 140.1 and 129.9 kcal/mol of energy, starting from *trans*- and *cis*-$B(OH)_3$(a), respectively. In our calculations, we observed significant results regarding the desorption energy of the OB(OH)O moiety on the Ti surface with two H atoms on different sides of the bridged oxygen atoms and with the two H atoms on the same side. Upon comparing both Figures 3e and 5k, the structures with H atoms on the different sides of bridged oxygens have a 10.2 kcal/mol higher desorption energy than the structure with the H atoms on the same side of the bridged oxygens.

Reaction Path for the Adsorption and Dissociation of the $B(OH)_3$ Dimer on the Surface. Similarly, Figures 6 and 7 show the potential energy diagrams and corresponding geometrical structures of two $B(OH)_3$ molecules on the TiO_2 anatase (101) surface. The associated bond lengths and the adsorption energies are listed in Table 3. We calculated all possible adsorbate structures of the two $B(OH)_3$ molecules on the surface and considered only the most stable conformation of the geometry given in Figure 7a, with an adsorption energy of 34.2 kcal/mol, which is nearly twice that of the monomer. In the most stable conformation, two $B(OH)_3$ molecules adsorbed side by side on the surface in a configuration like that of the monodentate, with hydroxyl oxygens attaching to two surface Ti_{5c} atoms, with two other hydroxyl groups forming hydrogen bonds to two bridged oxygen O_{2c} surface atoms shown as 2(O_b···HOB(OH)O(H)−Ti(a)) in Figure 7a. Their bond lengths are Ti−O2 = 2.278 Å, Ti−O6= 2.299 Å, and H···O_b = 1.683 and 1.659 Å.

Starting from the more stable adsorbate, 2(O_b···HOB-(OH)O(H)−Ti(a)) can isomerize without an intrinsic barrier to produce the intermediate hydrogen-bonding complex, which lies 1.7 kcal/mol above the stable adsorbate. As shown in Figure

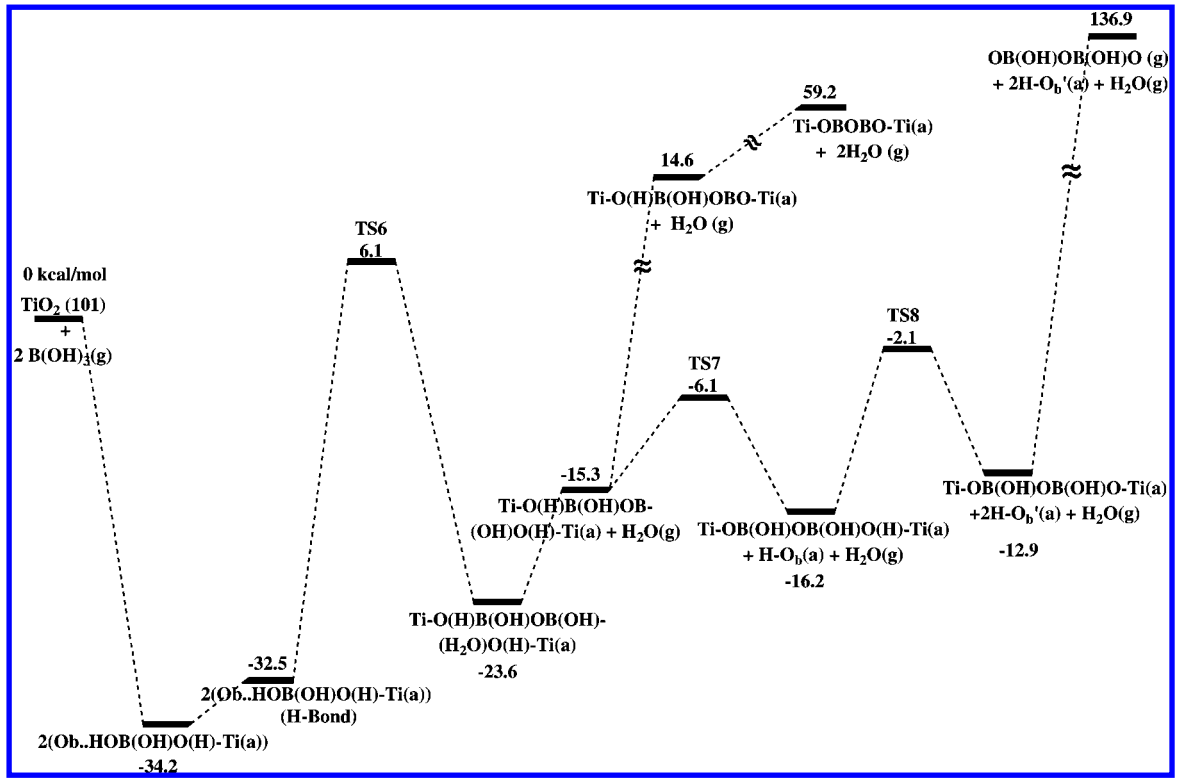

Figure 6. Potential energy surface of the surface reactions starting with the dimer of $B(OH)_3$(g) on the TiO_2(101) surface. (The ′ represents the two hydrogens adsorbed on different sides of the bridged oxygen rows; see Figure 7f.)

7b, one of the OH hydrogen atoms is hydrogen-bonded to the OH of its neighboring molecule with the O−H···O−H bond length of 2.733 Å. From the resulting intermediate, the H atom of the OH of one boric acid can react with one of the OH groups of another molecule intermolecularly to eliminate H_2O, producing the bidentate bridged water complex, Ti−O(H)B(OH)-OB(OH)(H_2O)O(H)−Ti(a), via **TS6**. The transition state of the H_2O-elimination process is located 6.1 kcal/mol above the initial reactants. This molecular elimination process is endothermic and requires 8.9 kcal/mol of energy. From this H_2O complex, it can eliminate the H_2O(g) from the surface to form a Ti−O(H)B(OH)OB(OH)O(H)−Ti(a) (see Figure 7d). The energy required is 8.3 kcal/mol, and the detailed bond lengths are given in Table 3.

Further restructuring can occur by two successive H migrations and successive H_2O elimination pathways. The first H migration from one of the surface-bonding O−H groups is an exothermic reaction involving the formation of a strong Ti−O bond and a H−O bond on a neighboring bridge oxygen. The breaking of the O−H bond occurs, and at the same time, the bond lengths between the borate O atom and the surface Ti atoms change from 2.321 to 1.851 Å. The migration of the H from the borate to bridging O atoms occurs with a 9.2 kcal/mol barrier at **TS7**, indicating the ease of the process forming Ti−OB(OH)OB(OH)O(H)−Ti(a) + H−O_b(a) (see Figure 7e). The transition state (**TS7**) of this reaction takes place with the formation of the O−Ti bond with a bond length of 1.851 Å, as mentioned above, and the O−H and H−O_b bond lengths of 1.236 Å and 1.193 Å, respectively, for breaking and forming, with a 0.9 kcal/mol energy drop. Following the similar H migration process, the second surface-bonding OH group in Ti−OB(OH)OB(OH)O(H)−Ti(a) can undergo the isomerization reaction via **TS8**, producing bidentate bridging Ti−OB(OH)OB-(OH)O−Ti(a) and 2H−O_b′(a) with a 14.1 kcal/mol activation barrier. The exothermicity of the process is predicted to be 12.9 kcal/mol when compared with the initial reactants. From Figure 7f, in Ti−OB(OH)OB(OH)O−Ti(a), the two terminal oxygens of the OB(OH)OB(OH)O moiety bind to the two Ti_{5c} atoms with O−Ti_{5c} bond lengths of about 1.937 and 1.879 Å, whereas the two hydrogens moves to two edge O_{2c} sites. The dissociation energy of the final product, Ti−OB(OH)OB(OH)O−Ti(a) → OB(OH)OB(OH)O(g) + 2H−O_b′(a) + H_2O(g), requires 149.8 kcal/mol (or without the spin polarization calculation, 169.3 kcal/mol), suggesting the very strong bonding between the $(HO)_2B_2O_3$ species with the protonated TiO_2 surface.

In the H_2O-elimination process from the resulting intermediate, Ti−O(H)B(OH)OB(OH)O(H)−Ti(a), which lies below the reactants by 15.3 kcal/mol, the H atom of one of the surface-bonding O−H groups can react with the OH group in the same O(H)BOH moiety to eliminate H_2O(g) intramolecularly, producing Ti−O(H)B(OH)OBO−Ti(a) via a barrierless and endothermic H_2O-complexation processes. The endothermicity is around 29.9 kcal/mol. Following the similar H_2O-elimination process in the adsorbate, the final products Ti−OBOBO−Ti(a) + 2H_2O(g) lie 59.2 kcal/mol above the reactants 2 $B(OH)_3$(g) + anatase TiO_2 (101).

Hydrogen Effect on Adsorbate Structures and Adsorption Energies. As demonstrated previously, H-atom adsorption on a neighboring O_b atom to both H_2O and HCOOH affects their binding energies. We report in this section on the effect of H(a) on the decomposed fragments of $B(OH)_3$. The optimized structures are shown in Figures 3 and 7, and related bond lengths and adsorption energies are listed in Tables 2 and 3. As mentioned previously, boric acid adsorbs on a clean TiO_2 surface to produce a monodentate conformation with an adsorption energy of 17.2 kcal/mol. The calculated adsorption energy of Ti−OB(OH)O(H)−Ti(a) is 28.0 kcal/mol (38.3 kcal/mol without spin) (see Figure 3l). Figure 3d shows that the coadsorption of hydrogen on a neighboring bridge oxygen in the Ti−OB(OH)-O(H)−Ti(a) has a much higher adsorption energy of 74.9 kcal/

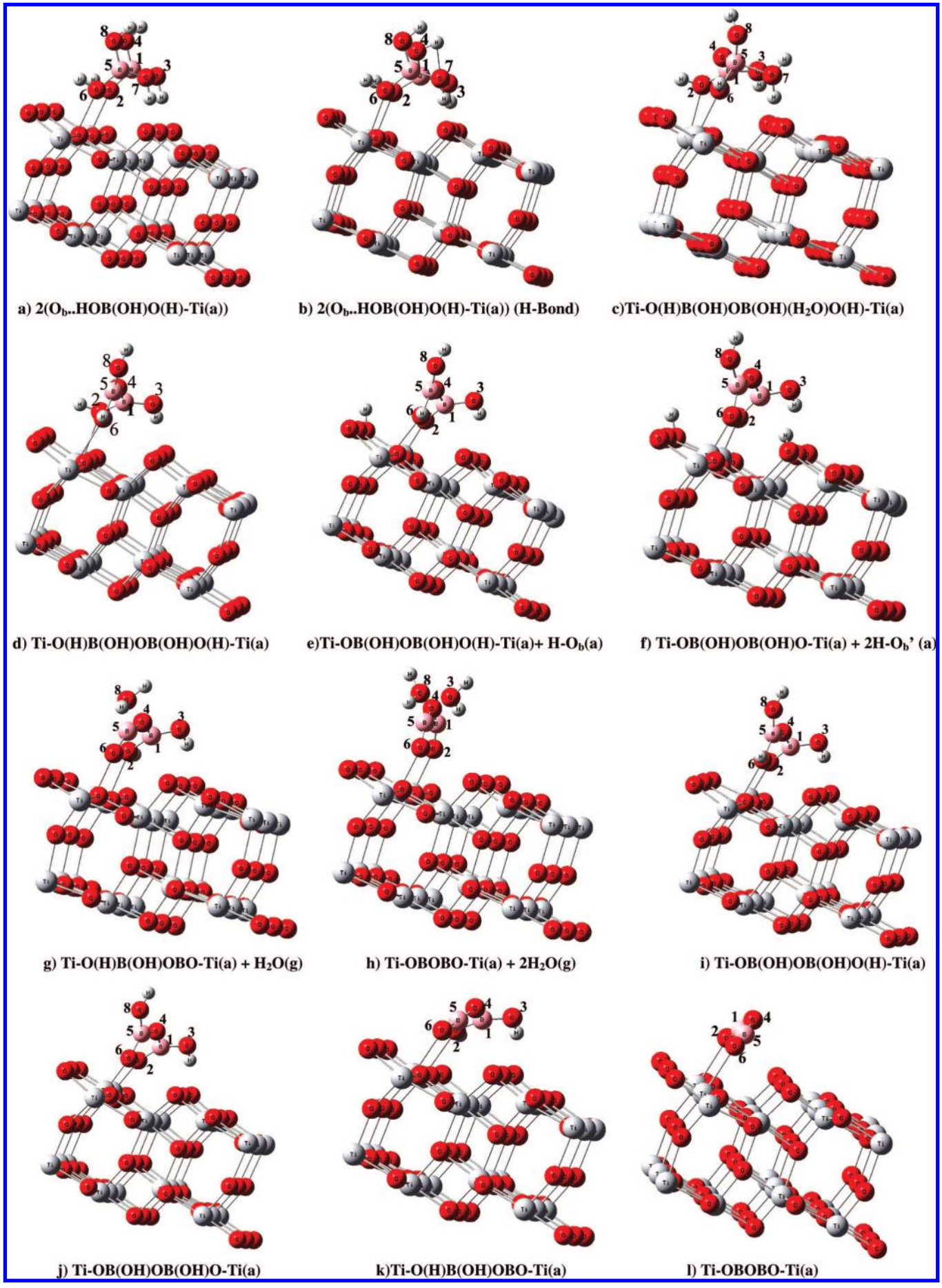

Figure 7. Optimized structures of possible adsorbed and dissociatively adsorbed dimer $B(OH)_3$ on the anatase (101) surface presented in Figure 6. (The ′ represents the two hydrogens adsorbed on different sides of the bridged oxygen rows.)

TABLE 3: Optimized Bond Lengths (Å) and Adsorption Energies (kcal/mol) for the $B(OH)_3$ Dimer and Its Fragments on the TiO_2(101) Surface

structure	Ti−O2	O2−B1	B1−O3	B1−O4	Ti−O6	O6−B5	B5−O7	B5−O8	B5−O4	OH−O_b	O_b−Ti_{6c}	E_{ads}
2(O_b···HOB(OH)O(H)−Ti(a))	2.278	1.412	1.342	1.373	2.299	1.413	1.341	1.372	−	1.683	1.898	34.2
2(O_b···HOB(OH)O(H)−Ti(a)) (H bond)	2.280	1.411	1.340	1.371	2.289	1.408	1.347	1.374	−	1.683	1.902	32.5
Ti−O(H)B(OH)OB(OH)O(H)−Ti(a)	2.321	1.401	1.345	1.371	2.332	1.396		1.366	1.354	3.081	1.865	22.1
Ti−OB(OH)OB(OH)O(H)−Ti(a)	1.887	1.357	1.364	1.384	2.297	1.404	−	1.372	1.343		1.840	34.4
Ti−OB(OH)OB(OH)O(H)−Ti(a)[a]	1.851	1.361	1.367	1.381	2.298	1.401		1.371	1.342		1.998	85.5
Ti−OB(OH)OB(OH)O−Ti(a)	1.937	1.361	1.364	1.379	1.879	1.358		1.367	1.381		1.858	44.3
Ti−OB(OH)OB(OH)O−Ti(a)′[b]	1.831	1.377	1.365	1.377	1.850	1.369		1.373	1.377		2.084	150.0
Ti−O(H)B(OH)OBO−Ti(a)	2.389	1.383	1.338	1.410	2.196	1.288	−	−	1.288		1.860	27.7
Ti−OBOBO−Ti(a)	2.424	1.216	−	1.324	2.471	1.212	−	−	1.327		1.862	14.7

[a] The adsorption is on the surface with one H(a) adsorbed on the anatase TiO_2(101) surface. [b] The adsorption is on the surface with two H(a) adsorbed on different sides on the anatase TiO_2(101) surface.

mol. The O_b atoms of these OH species have a Ti_{6c}−O distance of 2.116 Å compared with the value of 1.887 Å for the same adsorbate without hydrogen on the clean surface; these bond lengths are in good agreement with a previous finding.[33] Woodruff et al. in their experimental and theoretical studies showed the coexistence of formate, HCOO, and hydroxyl, OH, surface species. The hydroxyl species was formed by H attachment to the surface O_b atom and have a Ti−O bond length of 2.02 ± 0.05 Å, significantly longer than that of the bridging oxygen atoms on a clean TiO_2(110) surface.[33] For Ti−OB(OH)O−Ti(a) (see Figure 3m), with the adsorption energy of 30.3 kcal/mol (16.5 kcal/mol without spin), the two bond lengths between O and Ti atoms, O3−Ti and O2−Ti, are 1.964 and 1.896 Å, respectively. Similarly, the adsorption energy for the same molecule with two hydrogens on different sides of the bridging oxygens, Ti−OB(OH)O−Ti(a) + 2H−O_b′(a) (see Figure 3e) is as high as 140.1 kcal/mol. The adsorption energy for the same molecule with two hydrogens on the same side of the bridging oxygens is 129.9 kcal/mol (see Figure 3k). The bond lengths between the borate O atoms and Ti atoms of the surface, that is, O3−Ti and O2−Ti, are 1.876 and 1.864 Å, respectively. The bond angle O3B1O2 at the boron atom of the borate increases slightly from 120.9 to 122.5°. The adsorption of H on the bridging O atom leads to an increase of the O_b−Ti_{6c} bond length from 1.850 to 2.10 Å. There is hydrogen bonding between the bridged oxygen of H and the adsorbate OB(OH)O on the TiO_2, and their bond lengths are 2.553 Å for O3−HO_b and 2.584 Å for O2−HO_b. The effect of hydrogen bonding on the adsorbate can play a significant role in the adsorption energy.[35] The adsorption energies for the HOBO−Ti(a), O_b−B(OH)O−Ti(a), and H−O_b(a) are 21.7, 44.1, and 56.2 kcal/mol, respectively.

As mentioned previously, in the case of the dimer adsorption energies, the most stable structure for the monodentate configuration is 2(O_b···HOB(OH)O(H)−Ti(a)), with an adsorption energy of 34.2 kcal/ml and Ti_{5c}−O2 and Ti_{5c}−O6 bond lengths of 2.278 and 2.299 Å, respectively. The adsorption energy for the adsorbate on two Ti_{5c} sites on the clean surface, Ti−O(H)B(OH)OB(OH)O(H)−Ti(a), is 22.1 kcal/mol. For Ti−OB(OH)OB(OH)O(H)−Ti(a) (see Figure 7i), the bond lengths of the O atoms with the two adsorbed Ti_{5c} atoms, Ti−O2 and Ti−O6, are 1.887 and 2.297 Å, respectively, with an adsorption energy of 34.4 kcal/mol (without spin value 43.3 kcal/mol), as alluded to before. The geometry of the same Ti−OB(OH)OB(OH)O(H)−Ti(a) is stabilized by the coadsorption of a hydrogen on a neighboring bridging O atom, with an adsorption energy of 85.5 kcal/mol (93.9 kcal/mol with out spin). Figure 7j and f show the adsorbate structures of OB(OH)OB(OH)O and OB(OH)OB(OH)O without and with two coadsorbed hydrogen atoms on bridged oxygens with adsorption energies of 44.3 and 150.0 kcal/mol, respectively. Without spin calculations, the corresponding values are 64.0 and 169.3 kcal/mol. The bond lengths between the Ti_{5c}−O2 and Ti_{5c}−O3 in Figure 7j and f are 1.937 and 1.879 Å and 1.831 and 1.850 Å, respectively. The bond angle O1B4O5 at the boron atom decreases slightly from 139.5 to 136.0°. Finally, the adsorption of H on the bridging O atoms leads to an increase of O−Ti bond lengths from 1.858 and 1.837 Å to 2.084 and 1.998 Å, respectively. The hydrogen bonds between the two H's on the neighboring bridged O to adsorbate O (O_b−H···O) are 2.799 and 2.727 Å. The adsorbate structures of OB(OH)OB(OH)O have two coadsorbed hydrogen atoms on the same side of the bridged oxygens with an adsorption energy of 142.6 kcal/mol, and their structure is given in the Supporting Information Figure S3. These results indicate that two hydrogen atoms adsorbed on bridged oxygens on different sides are energetically quite more stable than those on the same side.

Bader Atomic Charges. We have calculated the Bader charges on the adsorbate of OB(OH)O and OB(OH)OB(OH)O on TiO_2 surfaces and the H coadsorbate on bridged oxygen, as shown in Figure 8. We compared the adsorbate structures of both OB(OH)O and two coadsorbed hydrogen atoms on bridged oxygens. Applying this method to these molecules, it is found that the H coadsorption increases the charge of the OB(OH)O [OB(OH)OB(OH)O] adsorbate by 0.28 *e* [0.26 *e*], where *e* is the magnitude of the charge on the electron. In Figure 8a, the charge of the bridged surface oxygen is −0.85 *e*, whereas in Figure 8b, the charge of the same surface oxygen with H on it is −1.22 *e* (on oxygen) and 0.70 *e* (on hydrogen), which shows the significant atomic charge changes in the adsorbates with and without hydrogens on the bridged oxygens. The OB(OH)O adsorbate with two hydrogens adsorbed on the same side of bridged oxygens is 0.03 *e* less charge than that with hydrogens on different sides. In the case of the OB(OH)OB(OH)O adsorbate, hydrogens adsorbed on surface oxygen on the same side is 0.04 *e* more than that with hydrogens on different sides. Detailed geometries of hydrogens adsorbed on the same side and their Bader charges are given in the Supporting Information Figure S3. Therefore, similar to the bonding mechanism between OB(OH)O and the surface, the bond shows covalent character, with a small amount of charge transfer. The charges on oxygen atoms of the adsorbate binding with Ti_{5c} show significant variations. There is a simultaneous increase of the charge on the O atoms with the two adsorbed Ti_{5c} atoms from −1.20 and −1.15 *e* to −1.19 and −1.30 *e* in Figure 8a and b, respectively. The resulting change in atomic charge is also very similar in the OB(OH)OB(OH)O case. The changes in the estimated Bader charges are consistent with the increase in the binding energies of both species OB(OH)O and OB(OH)OB(OH)O.

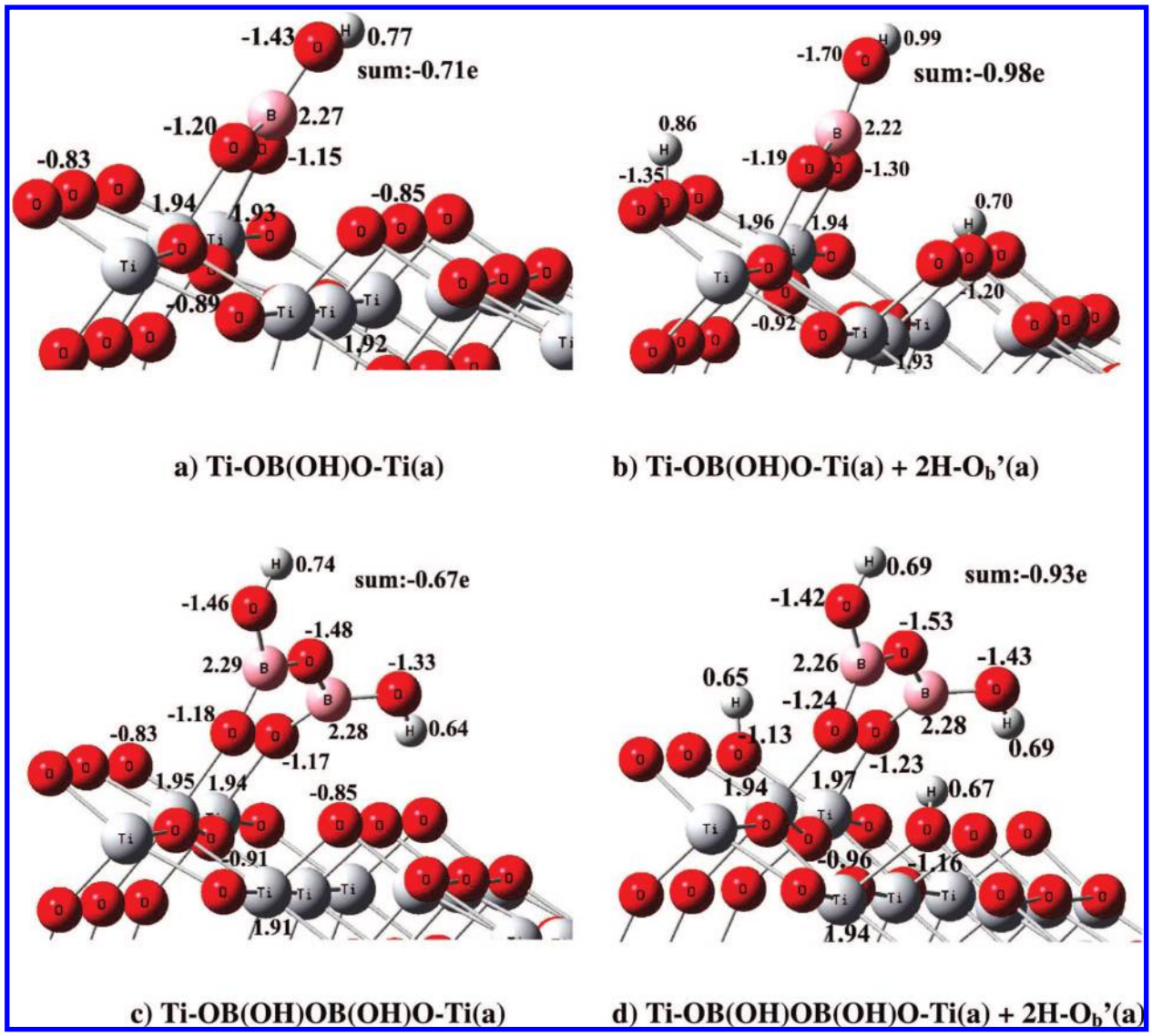

Figure 8. Bader atomic charges (*e*) on some important adsorbate molecules on the anatase (101) surface.

Conclusion

In this work, we have systematically studied the monomer and dimer of boric acid molecule adsorption and reactions on the anatase TiO_2(101) surface using first-principles calculations. The most stable adsorption structure for $B(OH)_3$ on the clean surface is a molecular monodentate configuration with one hydrogen bonded to a neighboring surface bridging oxygen; its adsorption energy is 17.2 kcal/mol. The resulting $O_b\cdots$ HOB(OH)O(H)−Ti(a) complexes are predicted to have large adsorption energies and are have the possibility to overcome the barriers for the H atom to migrate to a neighboring bridged oxygen, producing stable Ti−OB(OH)O−Ti(a) + 2H−O_b'(a) with an estimated exothermicity of 10.8 kcal/mol. Another product is the elimination of H_2O from this intermediate with a high energy barrier (57.4 kcal/mol) giving rise to the O_b−B(OH)O−Ti(a) adsorbate, which is endothermic by 5.9 kcal/mol.

A similar study on the reactions of $2B(OH)_3$ on the surface produces the two identical molecules like the monodentate configurations of $B(OH)_3$ adsorbed on two five-fold-coordinated Ti atoms of the anatase surface with an adsorption energy of 34.2 kcal/mol, which is almost two times that of the monodentate, reflecting a negligible adsorbate−adsorbate interaction because of the planar $B(OH)_3$ structure. Elimination of H_2O from the 2(Ob$\cdots$HOB(OH)O(H)−Ti(a)) complex required 38.6 kcal/mol of energy. Further decomposition into Ti−OB(OH)OB-(OH)O−Ti(a) and 2H−O_b'(a) is predicted to be exothermic by 12.9 kcal/mol. For the intermediate Ti−O(H)B(OH)OB(OH)-O(H)−Ti(a), the required activation energy for H migration from the bonding O−H groups is 9.2 kcal/mol for the first O−H breaking and 14.1 kcal/mol for the second O−H breaking. We found that dissociation reaction processes of boric acid on the anatase surface are energetically favorable. The final products of boric acid dissociative adsorptions Ti−OB(OH)O−Ti and Ti−OB(OH)OB(OH)O−Ti bond very strongly with the TiO_2 anatase surface with 140.1 and 150.0 kcal/mol binding energies, respectively, when H atoms are coadsorbed on their neighboring bridged surface O atoms. These species may be quite useful for interface linking between the semiconductor quantum dots such as InN and TiO_2 nanoparticles in the fabrication of solar cells.

Acknowledgment. The authors thank the Institute of Nuclear Energy Research (INER), Taiwan, for the funding of this project. M.C.L. acknowledges the support from the Taiwan Semiconductor Manufacturing Company for the TSMC Distinguished Professorship and from the National Science Council of Taiwan

for the Distinguished Visiting Professorship at National Chiao Tung University in Hsinchu, Taiwan. We are very much indebted to Taiwan's National Center for High-Performance Computing for the extensive CPUs needed in this work. We thank Y. R. Tzeng in INER for helping us in performing Bader's charge analysis.

Supporting Information Available: Optimized structures and Bader atomic charges. This material is available free of charge via the Internet at http://pubs.acs.org.

References and Notes

(1) Herman, G. S.; Dohnalek, Z.; Ruzycki, N.; Diebold, U. *J. Phys. Chem. B* **2003**, *107*, 2788.

(2) O'Regan, B.; Gratzel, M. *Nature* **1991**, *353*, 737.

(3) (a) Gratzel, M. *Nature* **2001**, *414*, 338. (b) Nazeeruddin, M. K.; Kay, A.; Rodicio, I.; Humphry-Baker, R.; Muller, E.; Liska, P.; Vlachopoulos, N.; Gratzel, M. *J. Am. Chem. Soc.* **1993**, *115*, 6382.

(4) Huisman, C. L.; Goossens, A.; Schoonman, J. *Chem. Mater.* **2003**, *15*, 4617.

(5) Li, D.; Gu, C.; Guo, C.; Hu, C. *Chem. Phys. Lett.* **2004**, *385*, 55.

(6) (a) Blackburn, J. L.; Selmarten, D. C.; Nozik, A. J. *J. Phys. Chem. B* **2003**, *107*, 14154. (b) Yu, P.; Zhu, K.; Norman, A. G.; Ferrere, S.; Frank, A. J.; Nozik, A. J. *J. Phys. Chem. B* **2006**, *110*, 25451.

(7) Vogel, R.; Hoyer, P.; Weller, H. *J. Phys. Chem.* **1994**, *98*, 3183.

(8) Shah, A.; Torres, P.; Tscharner, R.; Wyrsch, N.; Keppner, H. *Science* **1999**, *285*, 692.

(9) (a) Bu, Y.; Ma, L.; Lin, M. C. *J. Vac. Sci. Technol., A* **1993**, *11*, 2931. (b) Bu, Y.; Ma, L.; Lin, M. C. *Mater. Res. Soc. Symp. Proc.* **1993**, *335*, 21.

(10) (a) Wang, J. H.; Lin, M. C. *ChemPhysChem* **2004**, *5*, 1615. (b) Wang, J. H.; Lin, M. C. *J. Phys. Chem. B* **2006**, *110*, 2263. (c) Tzeng, Y.-R.; Raghunath, P.; Chen, S.-C.; Lin, M. C. *J. Phys. Chem. A* **2007**, *111*, 6781.

(11) Chen, J. T.; Hsiao, C. L.; Hsu, H. C.; Wu, C. T.; Yeh, C. L.; Wei, P. C.; Chen, L. C.; Chen, K. H. *J. Phys. Chem. A* **2007**, *111*, 6755.

(12) (a) Zabri, H.; Gillaizeau, I.; Bignozzi, C. A.; Caramori, S.; Charlot, M.-F.; Cano-Boquera, J.; Odobel, F. *Inorg. Chem.* **2003**, *42*, 6655. (b) Pechy, P.; Rotzinger, F. P.; Nazeeruddin, M. K.; Kohle, O.; Zakeeruddin, S. M.; Humphrybaker, R.; Gratzel, M. *J. Chem. Soc., Chem.Commun.* **1995**, 65. (c) Zakeeruddin, S. M.; Nazeeruddin, M. K.; Pechy, P.; Rotzinger, F. P.; HumphryBaker, R.; Kalyanasundaram, K.; Gratzel, M.; Shklover, V.; Haibach, T. *Inorg. Chem.* **1997**, *36*, 5937. (d) Gillaizeau-Gauthier, I.; Odobel, F.; Alebbi, M.; Argazzi, R.; Costa, E.; Bignozzi, C. A.; Qu, P.; Meyer, G. J. *Inorg. Chem.* **2001**, *40*, 6073. (e) Bae, E.; Choi, W.; Park, J.; Shin, H. S.; Kim, S. B.; Lee, J. S. *J. Phys. Chem. B* **2004**, *108*, 14093. (f) Nilsing, M.; Lunell, S.; Persson, P.; Ojamaee, L. *Surf. Sci.* **2005**, *582*, 49. (g) She, C.; Guo, J.; Irle, S.; Morokuma, K.; Mohler, D. L.; Zabri, H.; Odobel, F.; Youm, K.-T.; Liu, F.; Hupp, J. T.; Lian, T. *J. Phys. Chem. A* **2007**, *111*, 6832.

(13) Wang, C. K.; M.S Thesis, National Chiao Tung University, Taiwan, 2007.

(14) Chang, J.-G. ; Wang, J. H.; Lin, M. C. *Phys. Chem. A* **2007**, *111*, 6746.

(15) Vittadini, A.; Selloni, A.; Rotzinger, F. P.; Gratzel, M. *J. Phys. Chem. B* **2000**, *104*, 1300.

(16) Kresse, G.; Hafner, J. *Phys. Rev. B* **1993**, *47*, 558.

(17) Kresse, G.; Hafner, J. *Phys. Rev. B* **1994**, *49*, 14251.

(18) Kresse, G.; Furthmuller, J. *Comput. Mater. Sci.* **1996**, *6*, 15.

(19) Kresse, G.; Furthmuller, J. *Phys. Rev. B* **1996**, *54*, 11169.

(20) Cleperley, D. M.; Alder, B. J. *Phys. Rev. Lett.* **1980**, *45*, 566.

(21) Perdew, J. P.; Yang, Y. *Phys. Rev. B* **1992**, *45*, 244.

(22) Lee, C.; Yang, W.; Parr, R. G. *Phys. Rev. B* **1988**, *37*, 785.

(23) Perdew, J. P.; Chevary, J. A.; Vosko, S. H.; Jackson, K. A.; Penderson, M. R.; Singh, D. J.; Fiolhais, C. *Phys. Rev. B* **1992**, *46*, 6671.

(24) Monkhorst, H.; Pack, J. *Phys. Rev. B* **1967**, *13*, 5188.

(25) Henkelman, G.; Uberuaga, B. P.; Jo′nsson, H. *J. Chem. Phys.* **2000**, *113*, 9978.

(26) Mills, G.; Jonsson, H.; Jacobsen, K. W. In *Clasical and Quantum Dynamics in Condensed Phases*; Ciccotti, G., Berne, B. J., Coker, D. F., Eds.; World Scientific: Singapore, 1998; Chapter 16.

(27) Frisch, M. J. Trucks, G. W.; Schlegel, H. B.; Scuseria, G. E.; Robb, M. A.; Cheeseman, J. R.; Montgomery, J. A.; Jr Vreven, T.; Kudin, K. N.; Burant, J. C.; Millam, J. M.; Iyengar, S. S.; Tomasi, J.; Barone, V.; Mennucci, B.; Cossi, M.; Scalmani, G.; Rega, N.; Petersson, G. A.; Nakatsuji, H.; Hada, M.; Ehara, M.; Toyota, K.; Fukuda, R.; Hasegawa, J.; Ishida, M.; Nakajima, T.; Honda, Y.; Kitao, O.; Nakai, H.; Klene, M.; Li, X.; Knox, J. E.; Hratchian, H. P.; Cross, J. B.; Bakken, V.; Adamo, C.; Jaramillo, J.; Gomperts, R.; Stratmann, R. E.; Yazyev, O.; Austin, A. J.; Cammi, R.; Pomelli, C.; Ochterski, J. W.; Ayala, P. Y.; Morokuma, K.; Voth, G. A.; Salvador, P.; Dannenberg, J. J.; Zakrzewski, V. G.; Dapprich, S.; Daniels, A. D.; Strain, M. C.; Farkas, O.; Malick, D. K.; Rabuck, A. D.; Raghavachari, K.; Foresman, J. B.; Ortiz, J. V.; Cui, Q.; Baboul, A. G.; Clifford, S.; Cioslowski, J.; Stefanov, B. B.; Liu, G.; Liashenko, A.; Piskorz, P.; Komaromi, I.; Martin, R. L.; Fox, D. J.; Keith, T.; Al-Laham, M. A.; Peng, C. Y.; Nanayakkara, A.; Challacombe, M.; Gill, P. M. W.; Johnson, B.; Chen, W.; Wong, M. W.; Gonzalez, C.; Pople, J. A. *Gaussian 03*, revision C.02; Gaussian, Inc.: Wallingford, CT, 2004.

(28) (a) Henkelman, G.; Arnaldsson, A.; Jonsson, H. *Comput. Mater. Sci.* **2006**, *36*, 354. (b) Arnaldsson , A.; Tang, W.; Henkelman, G. Bader Charge Analysis. http://theory.cm.utexas.edu/bader/.

(29) Burdett, J. K.; Hughbanks, T.; Miller, G. J.; Richardson, J. W., Jr.; Smith, J. V. *J. Am. Chem. Soc.* **1987**, *109*, 3639.

(30) Vittadini, A.; Selloni, A.; Rotzinger, F. P.; Grätzel, M. *Phys. Rev. Lett.* **1998**, *81*, 2954.

(31) Beltran, A.; Sambrano, J. R.; Calatayud, M.; Sensato, F. R; Andrés, J. *Surf. Sci.* **2001**, *490*, 116.

(32) Egashira, M.; Kawasumi, S.; Kagawa, S.; Seiyama, T. *Bull. Chem. Soc. Jpn.* **1978**, *51*, 3144.

(33) (a) Kackell, P.; Terakura, K. *Surf. Sci.* **2000**, *461*, 191. (b) Sayago, D. I.; Polcik, M.; Lindsay, R.; Toomes, R. L.; Hoeft, J. T.; Kittel, M.; Woodruff, D. P. *J. Phys. Chem. B* **2004**, *108*, 14316. (c) Allegretti, F.; O'Brien, S.; Polcik, M.; Sayago, D. I.; Woodruff, D. P. *Phys. Rev. Lett.* **2005**, *95*, 226104. (d) Allegretti, F.; O'Brien, S.; Polcik, M.; Sayago, D. I.; Woodruff, D. P. *surf. Sci.* **2006**, *600*, 1487. (e) Woodruff, D. P.; Bradshaw, A. M. *Rep. Prog. Phys.* **1994**, *57*, 1029.

(34) Tachikawa, M. *J. Mol. Struct.: Theochem* **2004**, *710*, 139.

(35) (a) Zhao, J.; Li, B.; Jordan, K. D.; Yang, J; Petek, H. *Phys. Rev B.* **2006**, *73*, 195309. (b) Onda, K.; Li, B.; Zhao, J.; Jordan, K. D.; Yang, J.; Petek, H. *Science* **2005**, *308*, 1154.

JP711246B